

The correlation of peaks in the microwave background

Alan F. Heavens¹ and Ravi K. Sheth²

¹*Institute for Astronomy, University of Edinburgh, Blackford Hill, Edinburgh EH9 3HJ, U.K.*

²*MPI für Astrophysik, Karl Schwarzschild Str. 1, D85740 Garching b. München, Germany*

23 March 2021

ABSTRACT

We present accurate predictions of the correlation function of hotspots in the microwave background radiation for gaussian theories such as those predicted in most inflation models. The correlation function of peaks above a certain threshold depends only on the threshold and the power spectrum of temperature fluctuations. Since there are both potentially observable quantities in a microwave background map, there are no adjustable parameters in the predictions. These correlations should therefore provide a powerful test of the gaussian hypothesis, and provide a useful discriminant between inflation and topological defect models such as the cosmic string model. The correlations have a number of oscillatory features, which should be detectable at high signal-to-noise with future satellite experiments such as MAP and Planck.

Key words: cosmic background radiation - cosmology; theory - early Universe - large-scale structure of Universe.

1 INTRODUCTION

The microwave background radiation is principally a relic of the early Universe, containing information on the fluctuations present at a redshift of about 1000. Detailed knowledge of the fluctuations is extremely valuable as a tool for distinguishing structure formation theories. The main alternative to the microwave background for this purpose is the distribution of galaxies at the present day, or at moderate redshifts. The microwave background has two great advantages over galaxy redshift surveys. Firstly, one needs to make no assumptions about the relationship between galaxy clustering and mass clustering (the issue of bias), and secondly, the microwave background probes the Universe when the fluctuations were extremely small, so linear perturbation theory can describe the predicted fluctuations to high accuracy. Against these advantages must be offset the problems of foreground contamination and the technical difficulties of producing a high signal-to-noise, high-resolution map of large areas of sky. Future satellite experiments planned by ESA and NASA (Bersanelli et al. 1996, Jungman et al. 1996) will produce such maps, and these will allow the spectrum of temperature fluctuations to be measured with high accuracy. The primary goal of such experiments will be to determine a number of cosmological parameters, such as the density parameter Ω_0 , the Hubble constant, and the mix of species of dark matter, all of which, in inflationary theories, influence the detailed shape of the temperature power spectrum. In such theories, the temperature map is a random gaussian field, whose properties are determined by the power spectrum (or correlation function) alone. It is vitally important to test whether the map is indeed gaussian, as if it is not, the proposed parameter estimation method (e.g. Jungman et al. 1996) is invalid. In addition, a non-gaussian map of the primary temperature anisotropies would indicate a quite different structure formation scenario from the standard inflation model.

There are several ways to test the gaussian hypothesis, such as the 3-point function (e.g. Hinshaw et al. 1994, Falk, Rangarajan & Srednicki 1993, Luo & Schramm 1993, Gangui et al. 1994), the genus and Euler-Poincaré statistic (Coles 1989, Gott et al. 1990, Luo 1994b, Smoot et al. 1994), the bispectrum (Luo 1994a, Heavens 1998, Ferreira, Magueijo & Gorski 1998), studies of tensor modes in the CMB (Coulson, Crittenden & Turok 1994), and peak statistics (Bond & Efstathiou 1987, Kogut et al. 1995, Kogut et al. 1996). For all of these it is possible in principle to make predictions for gaussian fields, and each method has its advantages. The bispectrum is attractive because the error analysis can be done without recourse to numerical simulation, and can treat the twin problems of missing sky regions and correlated noise (Heavens 1998), albeit at large computational expense. In this paper we explore an alternative: the correlation function of peaks in the microwave background. This has the advantage of being readily calculable, and also we find that the predicted correlation functions have oscillatory features which are not obviously present in the temperature autocorrelation function. In much the same way as

the oscillations in the power spectrum allow high precision determinations of cosmological parameters, the peak correlation function oscillations should allow a high precision test of the gaussian hypothesis. In the latter case, the correlation function of peaks above any given threshold is completely determined once the power spectrum is known; there are no free parameters.

In this paper, we calculate the 2-point correlation function of peaks in a 2D gaussian field, for any given power spectrum. We make no approximations other than to compute the correlation function for small angular separations so we assume the sky is flat and translate the sky power spectrum to an analogous 2D spectrum. We follow the peak statistics methods developed initially by Peacock & Heavens (1985) and Bardeen et al. (1986).

The layout of the paper is as follows. In section 2 we describe the method, and in section 3 present the results and compare with an approximate correlation function method introduced by Bardeen et al. (1986). In section 4 we discuss the results and the possibilities for Planck and MAP.

2 METHOD

In this section, we compute the two-point correlation function of local maxima in 2D gaussian random fields. For small separations, this calculation should be accurately applicable to the clustering of peaks in the microwave sky (see Bond & Efstathiou (1987) for further discussion of this point). The calculation is laid out as follows: after some definitions, we compute the 12×12 covariance matrix for the 12 variables which are required to specify the two peaks. We then invert this matrix to obtain the multivariate gaussian distribution for the variables, then apply the peak constraint and integrate over the remaining variables to obtain the correlation function.

2.1 Peaks in 2D

We define the temperature fluctuation by $\delta(\mathbf{x}) \equiv T(\mathbf{x})/\bar{T} - 1$, and its 2D Fourier transform by $\delta_{\mathbf{k}} \equiv \int d^2\mathbf{k} \delta(\mathbf{x}) \exp(i\mathbf{k} \cdot \mathbf{x})$. The fluctuations are specified entirely by the power spectrum, $P(k)$, defined by

$$\langle \delta_{\mathbf{k}} \delta_{\mathbf{k}'} \rangle = (2\pi)^2 P(k) \delta^D(\mathbf{k} + \mathbf{k}') \quad (1)$$

where angle brackets indicate ensemble averages, and δ^D is a 2D Dirac delta function. We will require moments of the power spectrum, defining

$$\sigma_j^2 \equiv \frac{1}{(2\pi)^2} \int d^2\mathbf{k} P(k) k^{2j}, \quad (2)$$

and spectral parameters

$$\gamma \equiv \sigma_1^2 / (\sigma_0 \sigma_2) \quad \theta_* \equiv \sqrt{2} \frac{\sigma_1}{\sigma_2}. \quad (3)$$

At peaks, the 2D gradient $\delta_i \equiv \partial\delta/\partial x_i$ vanishes, and the eigenvalues of the second derivative matrix $\delta_{ij} \equiv \partial^2\delta/\partial x_i \partial x_j$ are all negative. Since δ_{ij} is symmetric, we are concerned with 6 independent numbers $\mathbf{v} = \{\delta, \delta_x, \delta_y, \delta_{xx}, \delta_{xy}, \delta_{yy}\}$ to specify a local maximum. For a gaussian field, the probability density function for the 12 variables $\mathbf{v} \equiv \{\mathbf{v}^{(1)}, \mathbf{v}^{(2)}\}$, evaluated at two points separated by a distance \mathbf{r} , is

$$p(\mathbf{v}_1, \mathbf{v}_2) = \frac{1}{(2\pi)^6 ||M||^{1/2}} \exp\left(-\frac{1}{2} v_i M_{ij}^{-1} v_j\right). \quad (4)$$

The covariance matrix is $M_{ij} \equiv \langle (v_i - \bar{v}_i)(v_j - \bar{v}_j) \rangle$, overlines indicate ensemble averages, and the summation convention is assumed. Note that $\bar{v}_i = 0$ in our case, and M_{ij}^{-1} is the i, j component of the inverse of M .

The number density of peaks is a sum of 2D Dirac delta functions, centred on peaks $\mathbf{x}_{pk,q}$:

$$n_{pk} = \sum_q \delta^D(\mathbf{x} - \mathbf{x}_{pk,q}) \quad (5)$$

In the vicinity of a peak, we may expand

$$\delta(\mathbf{x}) \simeq \delta(\mathbf{x}_{pk}) + \frac{1}{2} \sum_{i,j} \frac{\partial^2 \delta}{\partial x_i \partial x_j} (\mathbf{x} - \mathbf{x}_{pk})_i (\mathbf{x} - \mathbf{x}_{pk})_j \quad (6)$$

so

$$(\mathbf{x} - \mathbf{x}_{pk})_i \simeq \left(\frac{\partial^2 \delta}{\partial x_i \partial x_j} \right)^{-1} \frac{\partial \delta}{\partial x_j} \quad (7)$$

and the Dirac delta function in (5) is

$$\delta^D(\mathbf{x} - \mathbf{x}_{pk}) \simeq |\det \delta_{ij}| \delta^D(\delta_i). \quad (8)$$

The mean number density is

$$\begin{aligned} \langle n_{pk}(\mathbf{x}) \rangle &= \langle |\det \delta_{ij}| \delta^D(\delta_i) \rangle \\ &= \int d\delta d\delta_{xx} d\delta_{xy} d\delta_{yy} |\det \delta_{ij}| p(\delta, \delta_i = 0, \delta_{ij}) \end{aligned} \quad (9)$$

and the range of integration is set by the requirement that the eigenvalues of $-\delta_{ij}$ are all positive. These eigenvalues are

$$\lambda = \frac{1}{2} \left[-(\delta_{xx} + \delta_{yy}) \pm \sqrt{(\delta_{xx} - \delta_{yy})^2 + 4\delta_{xy}^2} \right]. \quad (10)$$

If we introduce the notation

$$\begin{aligned} \nu &\equiv \frac{\delta}{\sigma_0} \\ X &\equiv -\frac{(\delta_{xx} + \delta_{yy})}{\sigma_2} \\ Y &\equiv \frac{(\delta_{xx} - \delta_{yy})}{\sigma_2} \\ Z &\equiv \frac{2\delta_{xy}}{\sigma_2} \end{aligned} \quad (11)$$

then the conditions for a maximum are $X > 0$ and $Y^2 + Z^2 < X^2$. The determinant is

$$\det \delta_{ij} = \frac{X^2 - Y^2 - Z^2}{4\sigma_2^2}. \quad (12)$$

To compute the mean number density, we need the covariance matrix for the 6 variables specifying the field and its first and second derivatives. The non-zero components are $\langle \nu^2 \rangle = \langle X^2 \rangle = 1$; $\langle \nu X \rangle = \gamma$; $\langle Y^2 \rangle = \langle Z^2 \rangle = 1/2$; $\langle \delta_x^2 \rangle = \langle \delta_y^2 \rangle = \sigma_1^2/2$. The matrix can readily be inverted, and the integrations over Y , Z and X performed. The expression for the differential number density as a function of peak height, $n_{pk}(\nu)$ is given in Bond & Efstathiou (1987), equation (A1.9):

$$n_{pk}(\nu) = \frac{1}{(2\pi)^{3/2} \theta_*^2} \exp(-\nu^2/2) G(\gamma, \gamma\nu) \quad (13)$$

where

$$\begin{aligned} G(\gamma, x_*) &\equiv (x_*^2 - \gamma^2) \left\{ 1 - \frac{1}{2} \operatorname{erfc} \left[\frac{x_*}{\sqrt{2(1-\gamma^2)}} \right] \right\} + x_* (1 - \gamma^2) \frac{\exp \left[\frac{-x_*^2}{2(1-\gamma^2)} \right]}{\sqrt{2\pi(1-\gamma^2)}} + \\ &\frac{\exp \left[\frac{-x_*^2}{3-2\gamma^2} \right]}{\sqrt{3-2\gamma^2}} \left\{ 1 - \frac{1}{2} \operatorname{erfc} \left[\frac{x_*}{\sqrt{2(1-\gamma^2)(3-2\gamma^2)}} \right] \right\} \end{aligned} \quad (14)$$

The correlation function is obtained similarly. We find the covariance matrix for the 12 variables, invert it to find their probability distribution, and integrate subject to the constraints. The cross-correlation function of peaks of height ν_1 and ν_2 is then given by

$$\begin{aligned} 1 + \xi(r|\nu_1, \nu_2) &= \frac{1}{4\theta_*^4 n_{pk}(\nu_1) n_{pk}(\nu_2)} \int_{X_1=0}^{\infty} \int_{X_2=0}^{\infty} \int_{Y_1=-X_1}^{X_1} \int_{Y_2=-X_2}^{X_2} \int_{Z_1=-\sqrt{X_1^2-Y_1^2}}^{\sqrt{X_1^2-Y_1^2}} \int_{Z_2=-\sqrt{X_2^2-Y_2^2}}^{\sqrt{X_2^2-Y_2^2}} dX_1 dX_2 dY_1 dY_2 dZ_1 dZ_2 \times \\ &(X_1^2 - Y_1^2 - Z_1^2) (X_2^2 - Y_2^2 - Z_2^2) p(\nu_1, X_1, Y_1, Z_1, \delta_x^{(1)} = 0, \delta_y^{(1)} = 0, \nu_2, X_2, Y_2, Z_2, \delta_x^{(2)} = 0, \delta_y^{(2)} = 0). \end{aligned} \quad (15)$$

The correlation function for peaks above a certain threshold ν is obtained by adding two further integrations over ν_1 and ν_2 , and replacing the differential number densities $n_{pk}(\nu)$ in the denominator of (15) by numerically-evaluated integrals $n_{pk}(> \nu)$. The calculation of the covariance matrix and the joint probability distribution is rather technical, and so appears in an appendix.

3 RESULTS

In the flat-sky approximation, the power spectrum $P(k)$ which we require is related simply to the conventional power spectrum of spherical harmonic coefficients $C_\ell \equiv \langle |a_{\ell m}|^2 \rangle$, where $\delta T(\theta, \phi) \equiv \sum_{\ell m} a_{\ell m} Y_\ell^m(\theta, \phi)$ (Bond & Efstathiou 1987):

$$P(k) = C_\ell \quad \text{with } k \simeq \ell \quad (16)$$

We run CMBFAST (Seljak & Zaldarriaga 1996) to generate the power spectrum C_ℓ , and interpolate to obtain a continuous power spectrum $P(k)$. We model the beam with a gaussian of FWHM b , so multiply the power spectrum by a gaussian

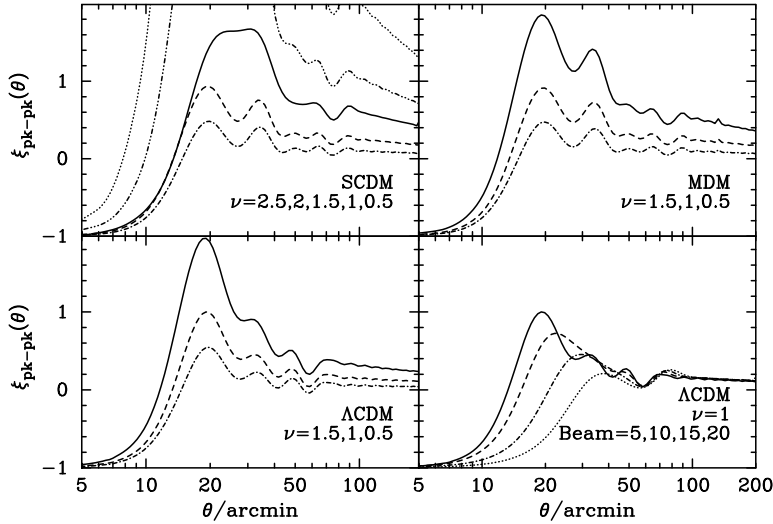


Figure 1. The correlation function of peaks in the microwave background, for a cold dark matter (CDM) model (top left; baryon density $\Omega_B = 0.05$, $\Omega_{CDM} = 0.95$), a mixed dark matter model containing hot dark matter (top right; $\Omega_B = 0.05$, $\Omega_{CDM} = 0.8$, $\Omega_{HDM} = 0.15$), and a flat cosmological constant model (bottom left; $\Omega_B = 0.05$, $\Omega_{CDM} = 0.15$, $\Omega_\Lambda = 0.8$). A Hubble constant $H_0 = 60 \text{ km s}^{-1} \text{ Mpc}^{-1}$ is assumed and the beam is 5 arcminutes FWHM. At bottom right, we show the effect on the cosmological constant model of altering the beam size. 5, 10, 15 and 20 arcminute beams are shown.

$\exp[-\sigma^2 \ell(\ell + 1)]$, with $\sigma = b/\sqrt{8 \ln 2}$. For peaks above a threshold, an 8D numerical integration is performed (although one could be done analytically), and, despite the integrand consisting of about 3000 lines of code, each point in the correlation function can be computed accurately in tens of seconds on a fast workstation.

In Fig. 1, we show the peak-peak correlation functions for a variety of models, for a 5 arcminute beam and peaks above various thresholds. The striking feature of these graphs is the wealth of structure in the correlation functions. The first peak is not due to the beam, rather due to the sharp turnaround in the power spectrum itself at around $\ell = 1500$, due to the thickness of the last scattering surface and/or Silk damping. There may be a correspondence in the peak positions with analogous peaks in the power spectrum, but it could also be ringing due to the abrupt cutoff. Note in particular that the temperature autocorrelation function (the Fourier transform of the power spectrum) is very smooth for these separations, without any oscillatory features. We also show in Fig. 1 the effect of beam-smearing. Correlation functions for beams of 5, 10, 15 and 20 arcminute are shown. The oscillations are more numerous and pronounced for smaller beam sizes, so it is advantageous to work at high resolution.

Later in this paper we will want to compute the correlations of estimates of the peak-peak correlation function. This is difficult analytically, so we have generated sky realisations, of 3072×3072 pixels, each 1 arcminute across, located local maxima, and computed the correlation function (see Fig. 2). Edge effects are irrelevant as we wrap the box round for pair counting. Fig. 3 shows the average of 10 such realisations, with the error on the mean plotted for each bin. The beam is 5 arcminutes and the spectrum is from a mixed dark matter model, which we have apodized with a cosine bell to remove power at long wavelengths. The apodizing affects $k < 30$, and is introduced to avoid discreteness errors arising at low- k from our continuum approximation used to evaluate the moments of the power spectrum and the $\lambda_{\alpha\beta\gamma}$, defined in the Appendix. Note the good agreement with the theoretical curve.

This numerical approach allows us to compute the correlation coefficients of the estimators $\hat{\xi}$ of the peak-peak correlation function. In Fig. 4 we show, from 100 realisations of a mixed dark matter model, $\langle (\hat{\xi}_i - \bar{\xi}_i)(\hat{\xi}_j - \bar{\xi}_j) \rangle / (\sigma_i \sigma_j)$ where $\bar{\xi}_i$ is the mean value and σ_i the variance of the estimates of the correlation function at radius r_i . These correlations would be required in order properly to quantify the significance of any departure from gaussian statistics. Note, however, that the correlation matrix is very close to diagonal, so distinct estimators are almost uncorrelated. We have also tested the approximate correlation function considered in 3D by Bardeen et al. (1986) and in 2D by Bond & Efstathiou (1987). In this approximation, more analytic progress is possible. The approximation ignores all derivatives of the temperature autocorrelation function, and it should be accurate for large separations. In the notation of the appendix, this means setting all the $\lambda_{\alpha\beta\eta} = 0$ except for the normalised autocorrelation function itself, λ_{000} . We show an example of the approximation, with the accurate solution, in Fig. 3. The approximation does quite well, especially at large separations, but fails to reproduce the oscillations. In Fig. 5, we show the expected errors from MAP and Planck for a mixed dark matter model. The data were obtained by repeatedly simulating part of the sky on a grid, and rescaling the errors to simulate 75% sky coverage. Details are given in the caption.

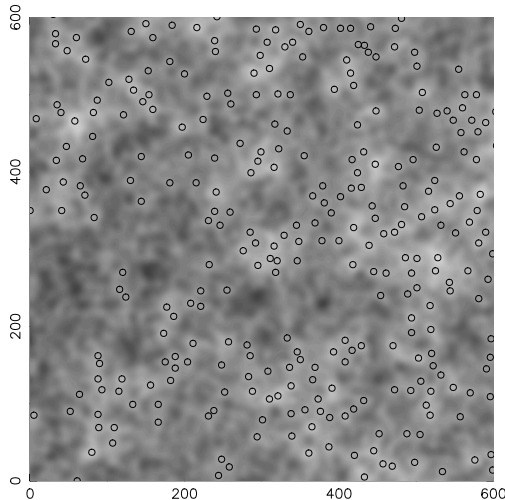


Figure 2. A $10^\circ \times 10^\circ$ patch of a mixed dark matter simulated sky, at 5 arcminute resolution characteristic of the highest frequency Planck channels. Peaks above 1σ are marked with circles.

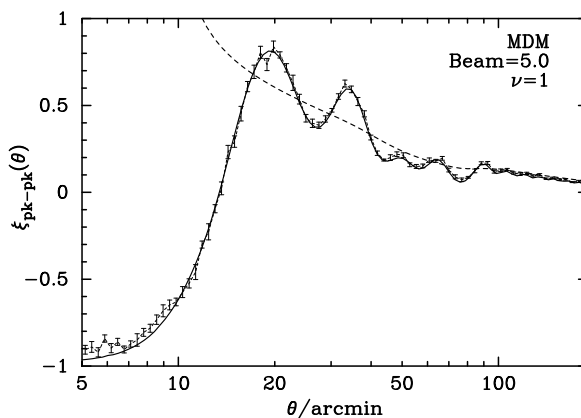


Figure 3. The $\nu = 1$ threshold from the mixed dark matter model in Fig. 1, with the correlation function from simulated gaussian fields superimposed. Also shown is the approximate correlation function computed by Bond & Efstathiou (1987) by ignoring derivatives of the temperature autocorrelation function.

4 DISCUSSION

In this paper we have shown that the peak-peak correlation function for the microwave sky can be computed to high accuracy for gaussian fields. The only approximation we make is that the sky is flat, but since the features in the correlation function appear on scales less than about 2 degrees, the computations should be very accurate. With upcoming high-resolution CMB experiments MAP and Planck, these results should allow a high-precision test of the hypothesis that structure grows from gaussian initial fluctuations, such as predicted in most inflationary models. We have not computed the expected peak-peak correlation function from defect models, but it is clear from the abundance of structure in the correlation function that agreement with these predictions, for all peak heights, would constitute a powerful argument in favour of gaussian models. We have also investigated numerically the errors expected from MAP and Planck; many of the features in the correlation function should be detectable with high significance. We note the similarity in the number of features in the peak-peak correlation function as in the power spectrum (although there may not be a simple correspondence between the two). The use of the two curves will, however, be rather different. To fit the power spectrum, one has the freedom to adjust fifteen or more parameters, under the gaussian hypothesis. With the peak-peak correlation function, there are no free parameters; for a gaussian process, all the statistics are specified once the power spectrum is fixed. Thus there is no freedom. Note also that the information

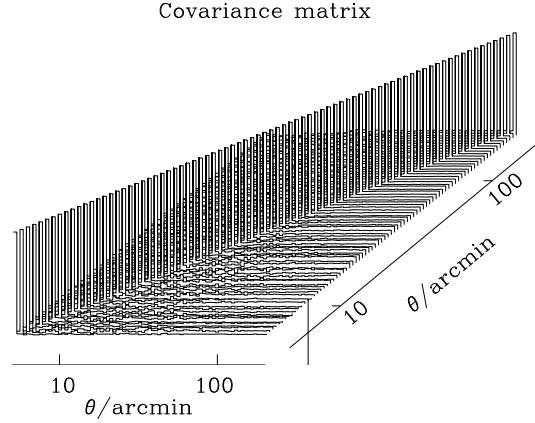


Figure 4. Correlation coefficients for estimators of the peak-peak correlation function of peaks above 1σ in the MDM simulation shown in Fig. 2.

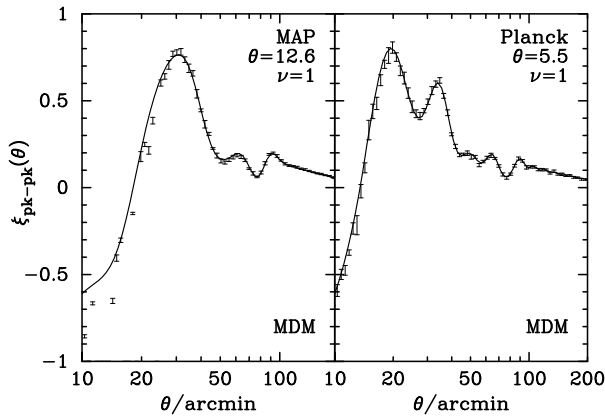


Figure 5. Mixed dark matter model correlation functions with errors expected from MAP (left) and Planck (right). The MAP simulations have a 12.6 arcminute beam, and Planck 5.5 arcminutes. Pixel sizes are taken to be 5 and 2 arcminutes. The simulations were done on square grids of side 3072 pixels, and the error bars (from run-to-run variations) rescaled to mimic 75% sky coverage. Note that the large pixels in MAP introduce discreteness errors for separations up to about 20 arcminutes, and the theoretical MAP curve is reliable only for separations greater than 15 arcminutes.

required for the gaussian test is just the power spectrum; it does not rely on a satisfactory parameter estimation. For practical purposes, there are some issues still to address; detector noise can be easily incorporated into the analysis provided it is gaussian. Practical de-stripping algorithms (e.g. Delabrouille 1998b, Revenu et al. 1998) to reduce $1/f$ noise, or methods to remove sidelobe contamination (Delabrouille 1998a) will need to be tested numerically to ensure that residual non-gaussian contributions are small. One interesting possibility for dealing with residual point sources in the maps is to put some constraint on the curvature at the peak (through the parameter x) to exclude sharply-peaked sources. The same trick could be used to exclude very flat-topped peaks whose precise locations may be difficult to determine accurately after dust foreground subtraction. Of course, both these techniques can be applied to the data as well as incorporated into the theory. There is an alternative to this procedure for point sources uncorrelated with the CMB; the peak distribution is then a superposition of two point processes, and provided the flux and clustering properties of the point sources are known, their contribution to the power spectrum can be subtracted. The gaussian test made on the joint distribution, as the correlation function will be a suitably-weighted combination of the two components. An aside which is probably not relevant for this application is that the analysis applies equally to any monotonic local functions of 2D gaussian fields, as nothing changes except the interpretation

of the threshold, although in general the non-gaussianity would be revealed in the one-point temperature distribution. In addition, one might expect any transformation process to be local in 3D, in which case the mixing of information through the last scattering surface would destroy the local nature.

APPENDIX

Joint distribution of variables

Consider two points separated by r . For convenience, place them on the x -axis. In the spirit of Regos & Szalay (1995), we define complex quantities

$$y_m^n(\mathbf{x}) \equiv \frac{i^n}{\sigma_n} \int d^2\mathbf{k} \delta_{\mathbf{k}} \exp(i\mathbf{k} \cdot \mathbf{x}) \exp(im\theta) k^n \quad (1)$$

where θ is the angle between \mathbf{k} and the x -axis. With this definition, $y_{-m}^n(\mathbf{x}) = y_m^{n*}(\mathbf{x})$. Then we require the following complex variables:

$$\begin{aligned} \sigma_0 y_0^0 &= \delta \\ \sigma_1 y_1^1 &= \delta_x + i\delta_y \\ \sigma_2 y_0^2 &= \delta_{xx} + \delta_{yy} \\ \sigma_2 y_2^2 &= \delta_{xx} + \delta_{yy} + 2i\delta_{xy} \end{aligned} \quad (2)$$

The correlations of these (at the same point) are

$$\langle y_m^n(\mathbf{x}) y_{m'}^{n'}(\mathbf{x}) \rangle = \frac{i^{n-n'}}{\sigma_n \sigma_{n'}} \int d^2\mathbf{k} d^2\mathbf{k}' \langle \delta_{\mathbf{k}} \delta_{\mathbf{k}'} \rangle \exp(i\mathbf{k} \cdot \mathbf{x} - i\mathbf{k}' \cdot \mathbf{x}) \exp(im\theta - im'\theta') k^{n+n'} \quad (3)$$

With the definition of the power spectrum (1), the integral simplifies to

$$\langle y_m^n(\mathbf{x}) y_{m'}^{n'}(\mathbf{x}) \rangle = \frac{i^{n-n'}}{\sigma_n \sigma_{n'}} \sigma_{(n+n')/2}^K \delta_{mm'} \quad (4)$$

where δ^K is the Kronecker delta. The cross-correlations between variables at \mathbf{x} and at $\mathbf{x} + \mathbf{r}$ are:

$$\langle y_m^n(\mathbf{x}) y_{m'}^{n'}(\mathbf{x} + \mathbf{r}) \rangle = \frac{i^{n-n'}}{\sigma_n \sigma_{n'}} \int d^2\mathbf{k} d^2\mathbf{k}' \langle \delta_{\mathbf{k}} \delta_{\mathbf{k}'} \rangle \exp(i\mathbf{k} \cdot \mathbf{x} - i\mathbf{k}' \cdot (\mathbf{x} + \mathbf{r})) \exp(im\theta - im'\theta') k^{n+n'}. \quad (5)$$

Inserting the power spectrum removes the \mathbf{k}' integration, leaving a 2D integration over \mathbf{k} . The angular part of this is

$$\begin{aligned} I_\theta &\equiv \int_0^{2\pi} d\theta \exp(-ikr \cos \theta) [\cos(m - m')\theta + i \sin(m - m')\theta] \\ &= 2\pi i^{|m-m'|} J_{|m-m'|}(-kr) \end{aligned} \quad (6)$$

where J is a Bessel function, and $J_\ell(-z) = (-1)^\ell J_\ell^*(z)$. Thus $\langle y_m^n(\mathbf{x} + \mathbf{r}) y_{m'}^{n'}(\mathbf{x}) \rangle = (-1)^{m+m'} \langle y_m^n(\mathbf{x}) y_{m'}^{n'}(\mathbf{x} + \mathbf{r}) \rangle$ and we find the cross-correlation matrix

$$\begin{pmatrix} \lambda_{000} & -\lambda_{020} & -\lambda_{011} & -\lambda_{011} & \lambda_{022} & \lambda_{022} \\ -\lambda_{020} & \lambda_{220} & \lambda_{121} & \lambda_{121} & -\lambda_{222} & -\lambda_{222} \\ \lambda_{011} & -\lambda_{121} & -\lambda_{110} & -\lambda_{112} & -\lambda_{121} & \lambda_{123} \\ \lambda_{011} & -\lambda_{121} & -\lambda_{112} & \lambda_{110} & \lambda_{123} & -\lambda_{121} \\ \lambda_{022} & -\lambda_{222} & -\lambda_{121} & -\lambda_{123} & \lambda_{220} & \lambda_{224} \\ \lambda_{022} & -\lambda_{222} & -\lambda_{222} & \lambda_{121} & \lambda_{224} & \lambda_{220} \end{pmatrix} \quad (7)$$

where the order of the variables is $\{y_0^0, y_0^2, y_1^1, y_1^{-1}, y_2^2, y_2^{-2}\}$ with quantities evaluated at \mathbf{x} down the left, and at $\mathbf{x} + \mathbf{r}$ along the top.

$$\lambda_{\alpha\beta\eta} \equiv \frac{(2\pi)^3}{\sigma_\alpha \sigma_\beta} \int dk k^{1+\alpha+\beta} P(k) J_\eta(kr) \quad (8)$$

We now make real variables

$$\begin{aligned} \nu &= y_0^0 \\ X &= -y_0^2 \\ Y &= \frac{1}{2}(y_2^2 + y_{-2}^2) \end{aligned}$$

$$\begin{aligned}
Z &= \frac{1}{2i}(y_2^2 - y_{-2}^2) \\
\eta_x &\equiv \frac{1}{2}(y_1^1 + y_{-1}^1) \\
\eta_y &= \frac{1}{2i}(y_1^1 - y_{-1}^1)
\end{aligned} \tag{9}$$

These definitions agree with (11) in the main text. The last two are $(\partial\delta/\partial x)/\sigma_1$ and $(\partial\delta/\partial y)/\sigma_1$. The entire correlation matrix for the variables in the order $(\nu_1, X_1, \eta_{x1}, Y_1, \nu_2, X_2, \eta_{x2}, Y_2, \eta_{y1}, \eta_{y2}, Z_1, Z_2)$ splits into an 8×8 matrix (top left)

$$M_8 \equiv \begin{pmatrix} 1 & \gamma & \cdot & \cdot & \lambda_{000} & \lambda_{020} & -\lambda_{011} & \lambda_{022} \\ \gamma & 1 & \cdot & \cdot & \lambda_{020} & \lambda_{220} & -\lambda_{121} & \lambda_{222} \\ \cdot & \cdot & 1/2 & \cdot & \lambda_{011} & \lambda_{121} & (\lambda_{110} - \lambda_{112})/2 & -(\lambda_{121} - \lambda_{123})/2 \\ \cdot & \cdot & \cdot & 1/2 & \lambda_{022} & \lambda_{222} & (\lambda_{121} - \lambda_{123})/2 & (\lambda_{220} + \lambda_{224})/2 \\ \lambda_{000} & \lambda_{020} & \lambda_{011} & \lambda_{022} & 1 & \gamma & \cdot & \cdot \\ \lambda_{020} & \lambda_{220} & \lambda_{121} & \lambda_{222} & \gamma & 1 & \cdot & \cdot \\ -\lambda_{011} & -\lambda_{121} & (\lambda_{110} - \lambda_{112})/2 & (\lambda_{121} - \lambda_{123})/2 & \cdot & \cdot & 1/2 & \cdot \\ \lambda_{022} & \lambda_{222} & -(\lambda_{121} - \lambda_{123})/2 & (\lambda_{220} + \lambda_{224})/2 & \cdot & \cdot & \cdot & 1/2 \end{pmatrix} \tag{10}$$

and a 4×4 block (bottom-right):

$$M_4 \equiv \begin{pmatrix} 1/2 & (\lambda_{110} + \lambda_{112})/2 & \cdot & -(\lambda_{121} + \lambda_{123})/2 \\ (\lambda_{110} + \lambda_{112})/2 & 1/2 & (\lambda_{121} + \lambda_{123})/2 & \cdot \\ \cdot & (\lambda_{121} + \lambda_{123})/2 & 1/2 & (\lambda_{220} - \lambda_{224})/2 \\ -(\lambda_{121} + \lambda_{123})/2 & \cdot & (\lambda_{220} - \lambda_{224})/2 & 1/2 \end{pmatrix} \tag{11}$$

Off-diagonal blocks are all zero. The 4×4 matrix is readily inverted. We used Mathematica to form the quadratic $v_i(M_8)_{ij}^{-1}v_j$ (where \mathbf{v} is the relevant part of the variable list, with the first derivatives set to zero). Since it produces several thousand lines of Fortran, it is not reproduced here.

REFERENCES

- Bardeen J. M., Bond J. R., Kaiser N., Szalay A. S., 1986. *ApJ*, 304, 15.
- Bersanelli M., Bouchet F., Griffin M., Lamarre J., Mandolesi N., Norgaard-Nielsen H., Pace O., Polny J., Puget J., Tauber J., Vittorio N., Volonté S., 1996. *ESA D/SCI*, 96, 3.
- Bond J. R., Efstathiou G. P., 1987. *MNRAS*, 226, 655.
- Coles P., 1989. *MNRAS*, 234, 509.
- Coulson D., Crittenden R., Turok N., 1994. *Phys. Rev. Lett.*, 73, 2390.
- Delabrouille J., 1998a. Ph.D. thesis, .
- Delabrouille J., 1998b. *A & A Suppl.*, 127, 555.
- Falk T., Rangarajan R., Srednicki M., 1993. *ApJ(Lett)*, 403, 1.
- Ferreira P., Magueijo J., Gorski K., 1998. *astro-ph*, 9803256.
- Gangui A., Lucchin F., Matarrese S., Mollerach S., 1994. *ApJ*, 430, 447.
- Gott J. R., Park C., Juskiewicz R., Bies W., Bennett D., Bouchet F., Stebbins A., 1990. *ApJ*, 352, 1.
- Heavens A. F., 1998. *MNRAS*, 299, 805.
- Hinshaw G., Kogut A., Gorski K., Banday A., Bennett C., Lineweaver C., Lubin P., Smoot G., Wright E., 1994. *ApJ*, 431, 1.
- Jungman G., Kamionkowski M., Kosowsky A., Spergel D. N., 1996. *Phys. Rev. D*, 54, 1332.
- Kogut A., Banday A., Bennett C., Hinshaw G., Lubin P., Smoot G., 1995. *ApJ*, 439, L29.
- Kogut A., Banday A., Bennett C., Gorski K., Hinshaw G., Smoot G., Wright E., 1996. *ApJ*, 464, L29.
- Luo X., Schramm D., 1993. *Phys. Rev. Lett.*, 71, 1124.
- Luo X., 1994a. *ApJ(Lett)*, 427, 71.
- Luo X., 1994b. *Phys. Rev.*, D49, 3810.
- Peacock J. A., Heavens A. F., 1985. *MNRAS*, 217, 805.
- Regos E., Szalay A. S., 1995. *MNRAS*, 272, 447.
- Revenu et al. B., 1998. in preparation, .
- Seljak U., Zaldarriaga M., 1996. *ApJ*, 469, 437.
- Smoot G. F., Tenorio L., Banday A., Kogut A., Wright E. L., Hinshaw G., Bennett C. L., 1994. *ApJ*, 437, 1.